## Supporting Information for

# Polyvinylpyrrolidone-enhanced perovskite films for efficient direct X-ray detection

Yanlong Hua,[a] Jiahui Chen,[b] Cuiling Guo,[a] Shan-Ci Chen,*[b] Yu He,*[a] and Huanghao Yang[a, c]

[a] *College of Chemistry, Fuzhou University, Fuzhou 350002, China. E-mail: heyu@fzu.edu.cn*

[b] *College of Materials Science and Engineering, Fuzhou University, Fuzhou 350116, P.R. China. E-mail: csc@fzu.edu.cn*

[c] *New Cornerstone Science Laboratory, MOE Key Laboratory for Analytical Science of Food Safety and Biology, College of Chemistry, Fuzhou University, Fuzhou 350002, China.*

# 1. Experiments

## 1.1. Chemicals and Reagents

Lead iodide ($PbI_2$, 99.999%), Methylammonium iodide (MAI, 99.999%), (6,6)-Phenyl $C_{61}$ Butyric Acid Methyl Ester ($PC_{61}BM$) and $SnO_2$ (12wt% in $H_2O$) were purchased from Xi'an Yuri solar Co., Ltd. Polyvinylpyrrolidone (PVP, Mw~55000) was purchased from Sigma-Aldrich. Chlorobenzene (CB, 99.8%), Dimethylformamide (DMF, 99.8%) and Dimethylsulfoxide (DMSO, 99.8%) were purchased from Thermo scientific. All commercial materials were used without any further purification.

## 1.2. Detector Fabrication

ITO glasses (2.0 × 2.0 cm) were initially cleaned with detergent, ultra-pure water, acetone, and isopropyl alcohol using ultrasonic, and then dried. Then the ITO glasses were subjected to UV ozone treatment for 15 minutes. $SnO_2$ colloidal dispersion was mixed with ultra-pure water in a volume ratio of 1:3. Then, the $SnO_2$ solution was filtered through a 0.45 μm filter and spin coated on the ITO substrates at 3000 rpm for 30 s, followed by annealing at 120 °C for 10 minutes and 150 °C for 20 minutes. The perovskite precursor solution was prepared by adding $PbI_2$ (2.5 M) and MAI (2.5 M) in the mixture of a DMF/ DMSO (9:1 by volume). Additionally, PVP was added to the solution as an additive at concentrations of 0 mg $mL^{-1}$, 3 mg $mL^{-1}$ and 5 mg $mL^{-1}$. Following stirring at 60 ℃ for 10 hours. The $SnO_2$-covered ITO substrate was treated with UV ozone for 15 minutes, and then heat it at 100 ℃. The 70 μL of perovskite precursor solution was dropped on the substrate hot plate, with a distance of 500 μm between the blade and the substrate. Finally, the blade was pushed at a speed of 10 millimeters $s^{-1}$ to evenly cover the solution on the substrate. After coating the blade, the resulting film was annealed at 120 °C for 10 hours. Finally, a 100 nm silver electrode was ultimately deposited on the surface of the perovskite film by thermal evaporation method. For electron-only devices, a PCBM layer was fabricated on the perovskite layer. A 20 mg $mL^{-1}$ PCBM solution was prepared using CB as the solvent and stirred at 70 °C for 2 hours. Subsequently, the PCBM solution (70 μL) was spin-coated onto the perovskite layer at 1500 rpm for 30 seconds, followed by annealing at 100 °C for 5 minutes.

## 1.3. Materials Characterizations

Photoluminescence (PL) emission spectra and PL decay curves (TRPL) were measured on the FLS980 spectrometer (Edinburgh) equipped with both continuous (450 W) and pulsed xenon lamps. A Rigaku MiniFlex-II X-ray diffractometer with Cu-Kα radiation (λ = 1.54184 Å) was used to record X-ray diffraction (XRD) patterns, with the films were placed at a scanning angle of 10 ° to 50 ° and a scanning speed of 10 ° $min^{-1}$. MAI and PVP (1:1 molar ratio) were dissolved in DMSO to prepare the experimental solution, and the same amount of PVP dissolved in DMSO to prepare the control solution. These solutions were analyzed by IS50R FTIR spectrometer to record Fourier transform infrared spectroscopy (FTIR). Field emission scanning electron microscopy (SEM, Nova Nano SEM 230 system) was used to detect the morphology of the surface cross-section of the film. X-ray photoelectron spectroscopy (XPS) was used to study the surface chemical state of the materials. The experiments were performed using an ESCALABQXI photoelectron spectrometer equipped with a monochromatic Al-Ka (1486.6 eV) X-ray source. During the analysis process, we corrected the electrostatic effects of all recorded peaks by calibrating the CAC component of the C 1s peak to 284.8 eV. The liquid state $^1$H nuclear magnetic resonance ($^1$H NMR) spectra was measured by a nuclear magnetic resonance spectrometer (BRUKERAV600).

## 1.4. Detector Performance Measurement

Tungsten anode X-ray tube (Moxtek MAGPRO) is used as a radiation source. The X-ray source operates at an acceleration voltage of 10 kV. The dose rate is controlled by varying the X-ray tube current and calibrated it using a Radcal ion chamber (model: 10 X 6-180) dosimeter. The current-voltage and X-ray response curves of the device are recorded at room temperature by using a customized X-ray detector electrical performance testing system. All X-ray response characterizations were performed in dark air to minimize interference from ambient light response.

## 2. Other Related Figures

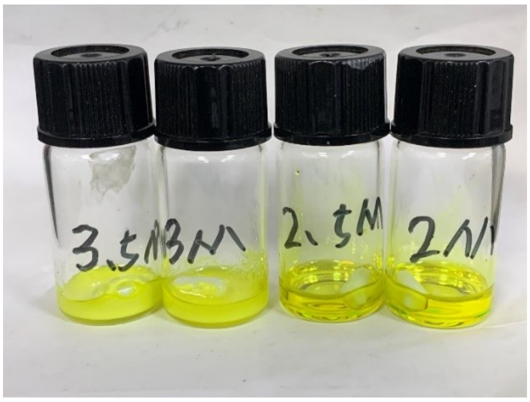

**Fig. S1.** A comparative dissolution diagram of precursor solutions with concentrations of 2.0 M, 2.5 M, 3.0 M, and 3.5 M, obtained after stirring at 60 °C for 12 hours.

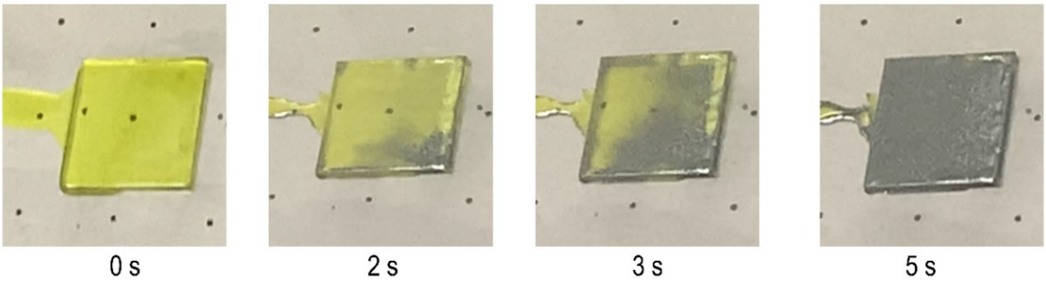

**Fig. S2.** Photographs of the change process of perovskite precursor solution on the substrate after blade coating under the ambient conditions (60%-70% humidity, 25 °C).

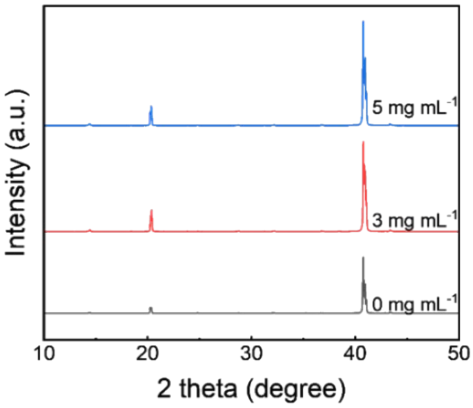

**Fig. S3.** XRD patterns of perovskite films with different concentrations of PVP.

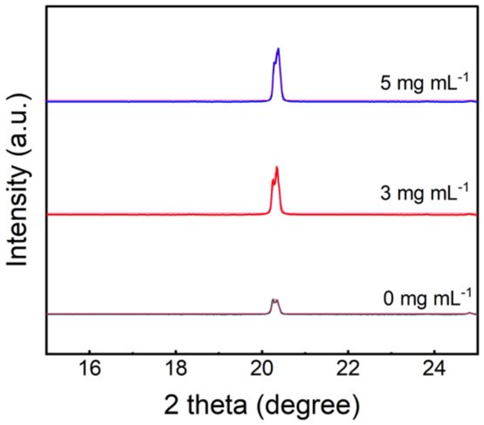

**Fig. S4.** Gaussian fitting plots of the maximum full-width at half-maximum (FWHM) for the (200) diffraction peaks of the three perovskite films within the diffraction angle range of 15° to 25°.

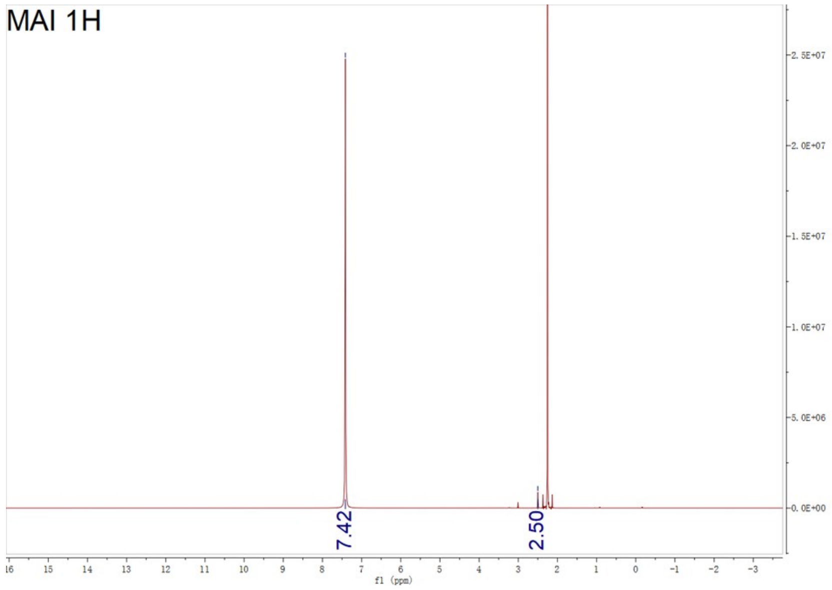

**Fig. S5.** $^1$H NMR full spectrum of MAI in DMSO-d6.

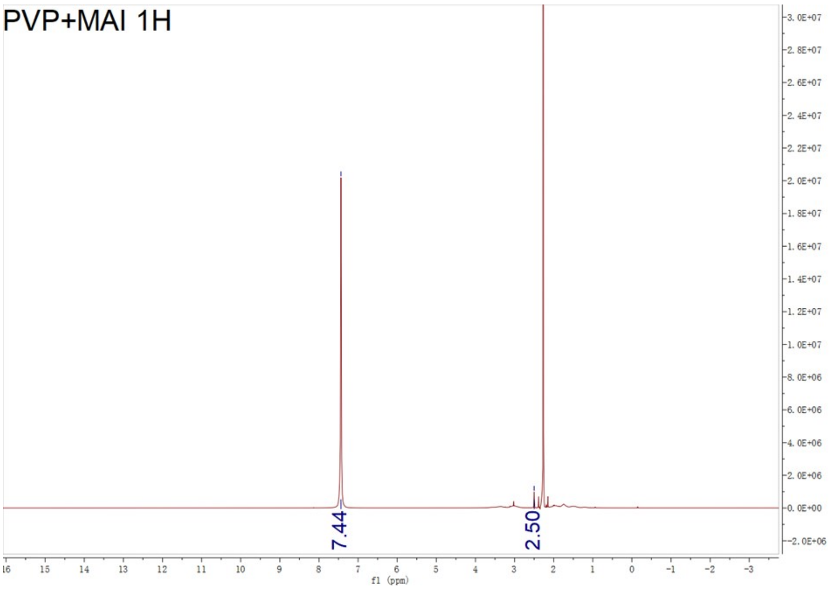

**Fig. S6.** $^1$H NMR full spectrum of PVP+MAI at a molar ratio of 1:1 in DMSO-d6.

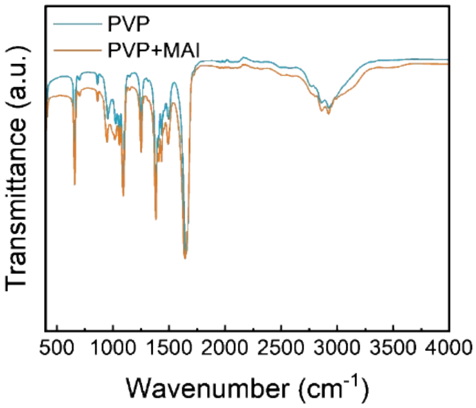

**Fig. S7.** FTIR full spectra of MAI, PVP+MAI prepared by mixing PVP with MAI in a molar ratio of 1:1.

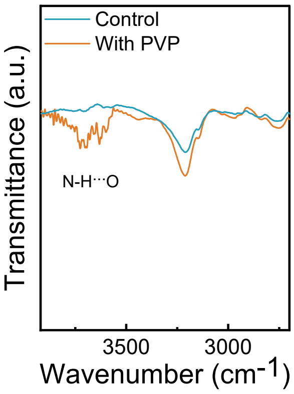

**Fig. S8.** FTIR spectra of control film and PVP-optimized film, a distinct peak at 3630 cm$^{-1}$ indicated the stretching vibration peak of N-H···O.

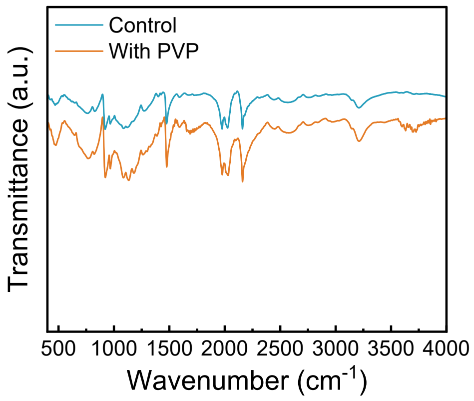

**Fig. S9.** FTIR full spectra of control film and PVP-optimized film.

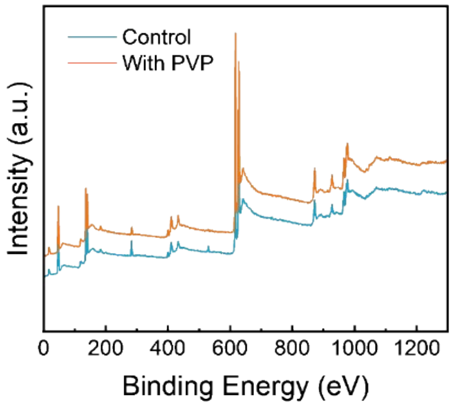

**Fig. S10.** XPS full spectra of control perovskite film and perovskite film with PVP.

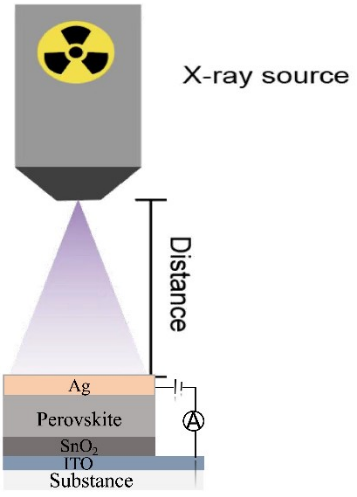

**Fig. S11.** Schematic diagram of device setup for X-ray performance test.

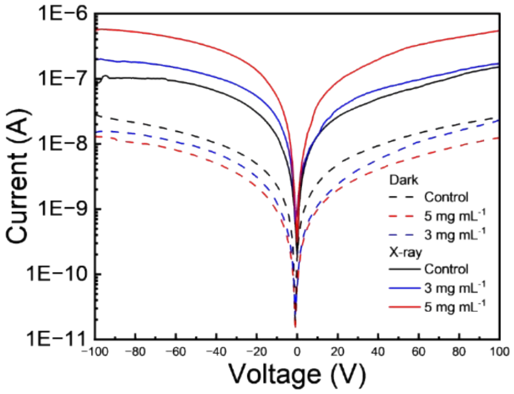

**Fig. S12.** Current voltage (*J*–*V*) curves of the detectors based on the films with different concentrations of PVP under dark condition and X-ray irradiation, the dose rate is 11470 µ$Gy_{air}$ $s^{-1}$.

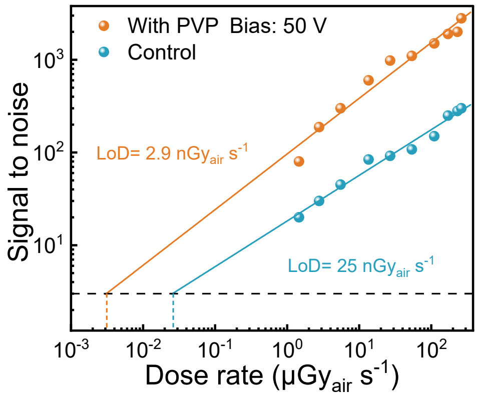

**Fig. S13.** Signal-to-noise ratio of the two detectors under bias voltages of 50 V and 10 keV X-ray energy. The dashed line means a SNR value of 3.

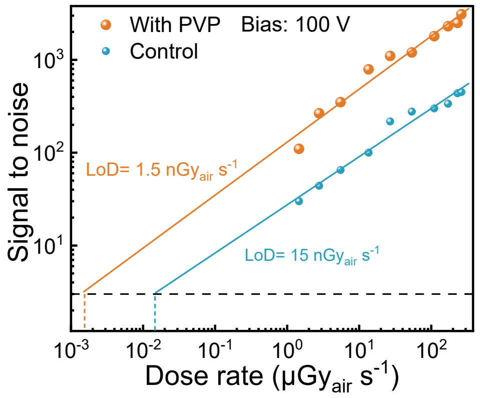

**Fig. S14.** Signal-to-noise ratio of the two detectors under bias voltages of 100 V and 10 keV X-ray energy. The dashed line means a SNR value of 3.

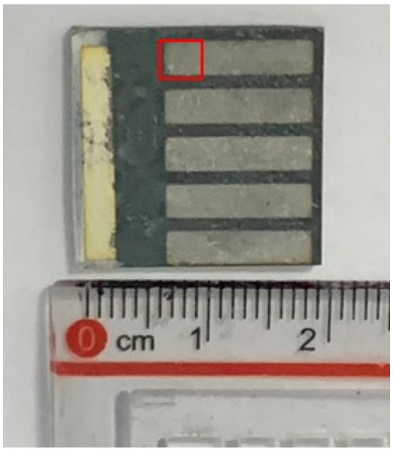

**Fig. S15.** Photograph of the complete device with an area of 2.0×2.0 cm, where the red box indicated the active device regions, totaling five active device regions.

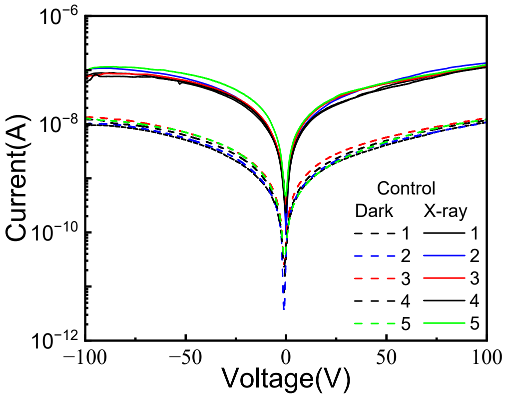

**Fig. S16.** *J–V* curves of the control detector under dark and X-ray radiation.

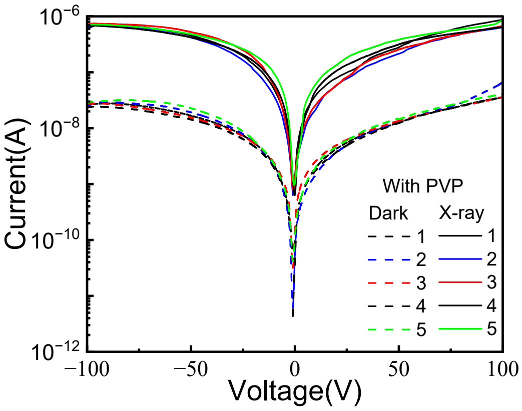

**Fig. S17.** *J–V* curves of the PVP-optimized detector under dark and X-ray radiation.

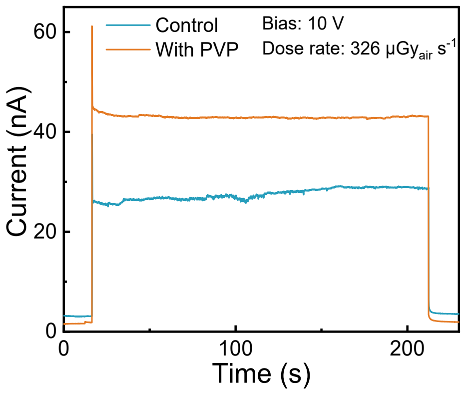

**Fig. S18.** Radiation stability of the two devices under a bias voltage of 10 V and X-ray energy of 10 keV.

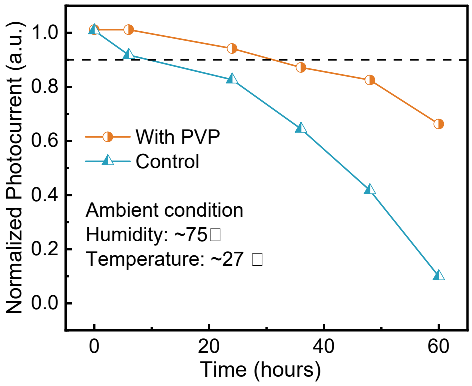

**Fig. S19.** The trend of X-ray current intensity of the device decreasing with storage time in ambient environment.

## Supplementary Note 1: Estimation of the upper sensitivity limit under 10 keV X-rays.

The upper theoretical limit of the specific surface sensitivity $S_{max}$ (μC Gy$^{-1}$ cm$^{-2}$) of a detector can be calculated by the following formula:

$$S_{max} = \frac{e\mu_P \rho d}{\mu E_i}$$

Here, *e* is the electron charge (C), *ρ* is the density of the active layer (g cm$^{-3}$), *d* is the thickness of the active layer (cm), $\mu_P$ and $\mu$ (cm$^2$ g$^{-1}$) are respectively the mass attenuation coefficients of the active layer material and dry air at the average photon energy. $E_i$ is the generation energy of electron-hole pairs, which can be expressed as $E_i$=2$E_g$ +1.43=4.43 eV (where $E_g$ is the band gap energy).

In the case of the device introduced in this work, the active material is a $MAPbI_3$ film with thickness d= 1.9×10$^{-3}$ cm. We assume the density of the $MAPbI_3$ active layer is = 4.1 g cm$^{-3}$, whereas $\mu_P$ and μ are obtained by using the XCOM software provided by NIST (National Institute of Standards and Technology). Fig S20 and Fig S21 reports the mass attenuation coefficient of $MAPbI_3$ and dry air in the 1 keV-10 MeV energy range.

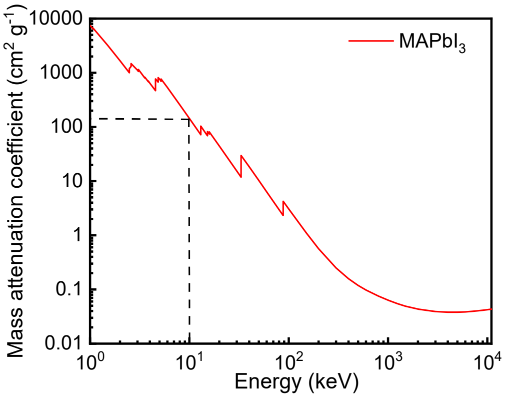

**Fig. S20.** Mass attenuation coefficient of $MAPbI_3$ in the 1 keV-10 MeV energy range.

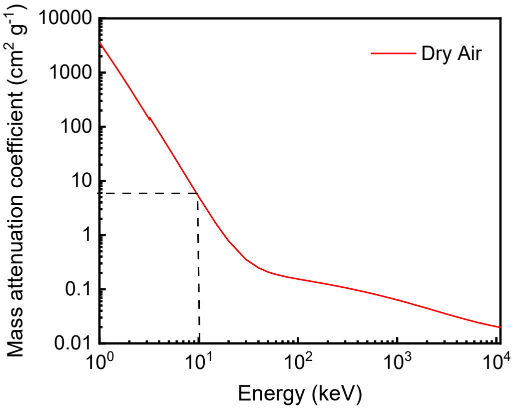

**Fig. S21.** Mass attenuation coefficient of dry air in the 1 keV-10 MeV energy range.

By considering a photon energy is 10 keV, the mass attenuation coefficient is $\mu_P$ = 139.96 cm$^2$ g$^{-1}$. At the same photon energy (10 keV), the mass attenuation coefficient of dry air is μ =6.06 cm$^2$ g$^{-1}$. Finally, being the bandgap energy $E_g$=1.5 eV, the estimated electron-hole pair creation energy is $E_i$=4.43 eV.

By substituting all the numerical values into the $S_{max}$ equation we obtain: $S_{max}$=40.61 μC Gy$^{-1}$ cm$^{-2}$

## 3. Other Related Tables

**Table S1.** The maximum full-width at half - maximum (FWHM) of the (200) diffraction peak of the three perovskite films in the diffraction angle range of 15°-25° was obtained through gaussian fitting.

| Model | Gauss | | |
|---|---|---|---|
| Equation | y=y0 + (A/(w*s qrt(Pi/2)))*exp( -2*((x-xc)/w)^2 ) | | |
| Sample | 0 mg mL$^{-1}$ | 3 mg mL$^{-1}$ | 5 mg mL$^{-1}$ |
| y0 | 1504.98808 | 2904.22154 | 2738.93775 |
| xc | 20.30719 | 20.32328 | 20.3504 |
| w | 0.14349 | 0.13961 | 0.13508 |
| A | 3625.64454 | 10485.79222 | 12100.62541 |
| sigma | 0.07174 | 0.06981 | 0.06754 |
| FWHM(β) | 0.16894 | 0.16438 | 0.15904 |
| Height | 20161.10268 | 59926.99632 | 71476.66866 |
| Reduced Chi-Sqr | 1.41540E6 | 1.21155E7 | 9.28510E6 |
| Adj. R-Square | 0.95177 | 0.95153 | 0.9743 |

**Table S2.** Detailed fitting parameters of the control $MAPbI_3$ film and $MAPbI_3$ film with PVP preparing on glass substrate, obtained from the TRPL measurement.

| Sample | $\tau_1$ [μs] | $B_1$ | $\tau_2$ [μs] | $B_2$ | $\tau_{ave}$ [μs] |
|---|---|---|---|---|---|
| Control | 0.77 | 0.82 | 9.51 | 0.03 | 3.49 |
| With PVP | 0.94 | 0.93 | 13.43 | 0.04 | 5.69 |

TRPL can be well fitted by the following formulas with biexponential components:

$$f(t) = A + B_1 exp(\frac{-t}{\tau_1}) + B_2 exp(\frac{-t}{\tau_2})$$

$$\tau_{ave} = \frac{B_1\tau_1^2 + B_2\tau_2^2}{B_1\tau_1 + B_2\tau_2}$$

where $A$ is a constant for the baseline offset, $B_1$ and $B_2$ are the relative amplitudes, $\tau_1$ and $\tau_2$ are the carrier lifetimes for the fast and slow recombination, respectively. $\tau_{ave}$ is average carrier lifetime.

**Table S3.** X-ray detection performance of this work in comparison with previous reports.

| Material | Sensitivity (μC $Gy_{air}^{-1}$ $cm^{-2}$) | LoD (n$Gy_{air}$ $s^{-1}$) | Bias voltage(V) | Thicknees (μm) | Reference |
|---|---|---|---|---|---|
| PVP/$MAPbI_3$ | 2.6×10$^3$ | 11 | 100 | 19 | This work |
| $PEA_2PbBr_4$ | 2998 | 0.79 | 100 | 1000 | S1 |
| $Cs_3Bi_2I_9$ | 1652.3 | 130 | 60 | 1200 | S2 |
| $Cs_2AgBiBr_6$ | 105 | 59.7 | 50 | 2000 | S3 |
| $(F\text{-}PEA)_2PbI_4$ | 3402 | 23 | 266 | 2000 | S4 |

## Reference

S1. Su X, Wang R, Yu H. Coatings, 2024, **14**, 633.

S2. Wang J, Zhang J, Zhou Y. Nature communications, 2020, **11**, 177.

S3. Pan W, Wu H, Luo J. Nature photonics, 2017, **11**, 726-732.

S4. Li H, Song J, Pan W. Advanced Materials, 2020, **32**, 2003790.